applied optics

Small-size, high-resolution angular displacement measurement technology based on an imaging detector

Hai Yu,* Qiuhua Wan, Xinran Lu, Yingcai Du, and Shouwang Yang

Changchun Institute of Optics, Fine Mechanics and Physics, Chinese Academy of Sciences, Changchun 130033, China
**Corresponding author: yuhai5158@163.com*

Received 20 October 2016; revised 21 December 2016; accepted 22 December 2016; posted 23 December 2016 (Doc. ID 279202); published 19 January 2017

It is challenging to design a photoelectric encoder that is small in size while ensuring it has sufficiently high resolution and accuracy. Traditional displacement measurement via the moiré fringe signal does not facilitate high resolution at small grate sizes; photoelectric and digital photo processing can significantly improve the angle measurement resolution over traditional techniques. The primary focus of this paper includes grating displacement coding and decoding, as well as the corresponding high-resolution subdivision and measurement error factors. A small-size absolute photographic encoder was designed (50 mm diameter) that exhibits resolution of 1.24″ (20 bit) with a standard deviation of error of 14.3″. The results presented here may provide a theoretical and technological foundation for further research on small-size, high-resolution photographic rotary encoders.

OCIS codes: (120.0280) Remote sensing and sensors; (130.6010) Sensors; (120.3930) Metrological instrumentation.

https://doi.org/10.1364/AO.56.000755

1. INTRODUCTION

High-resolution and high-precision rotary displacement measurement technology has been a popular research area in recent years [1–4]. The main factor that limits measurement resolution in photoelectrical rotary encoders is the size of the circular grating. The absolute encoder designed by the Heidenhain Company, which has a large circular grating, can reach 27 bit resolution [5]; a likewise large in size, ultrahigh-resolution absolute encoder was designed by the Goddard Space Center as optical pattern recognition and image processing technology [6]. Traditional encoding methods involve carving several lines in a single circle of grating to improve the measurement resolution when the grate size is small. An excessive number of lines have two main effects:

- Too many lines render the light flux insufficient and prevent accurate decoding;
- Lines that are too dense cause interference between adjacent grating grooves and impede angular division.

In recent years, we have seen remarkable developments in digital image processing techniques and devices [7–10]. Angular displacement measurement can be performed at higher resolution using an image detector rather than with the traditional moiré fringe method [11]. Many researchers have explored various image encoders in regards to their practical application. The most representative of these is the absolute encoder designed by NASA, which features resolution up to 0.01″ and linear displacement up to 0.01 μm [12,13]. In another landmark study, the Faculty of Science and Technology at Novi Sad (Serbia) proposed a device for measuring angular positions based on color identification; its resolving power is 0.1° and the linearity error is 1° [14]. The Hamamatsu Company (Japan) created an absolute shaft encoder based on an area-array detector that can reach 14 bit resolution [15]. Lleida University (Spain) used a CMOS sensor and an optical mouse to obtain image information and a microprocessor for angle measurement, effectually developing a high-resolution system that is very low in cost [16]. The Standards and Science Institution (Korea) developed an absolute angle measurement method that uses a 10 bit or 13 bit phase-shift coded disk with maximum angle measurement errors of 25″ and 4″, respectively, and a response frequency of 500 Hz [17]. The modern optical instrument laboratory at Zhejiang University (China) submitted a subdivision absolute-type encoder based on the area-array detector; its resolution can reach 0.011° [18]. Nanjing University of Science and Technology (NUST) (China) designed an image-encoder-based angular measuring system for electronic theodolite; the code disk is 79 mm, and the resolution is 1″ [19]. The Changchun Institute of Optics Fine Mechanics and Physics, Chinese Academy of Sciences (China) designed an

image encoder in 2013 that uses a CMOS area-array detector to recognize and compute encoder patterns; the resolution can reach 5″, and the maximum angle measurement error is 61″ [20].

A few notable conclusions can be drawn based on careful review of the literature. In summary, (1) previous studies neglect the frequency response of the photographic encoder; (2) most studies only explore decoding methods using imaging detectors, while there are relatively few studies on subdivisions; and (3) high resolution and high precision are very difficult to achieve at smaller grate sizes.

We conducted this study to explore the implementation of high-resolution measurement using a photographic encoder with a small grate. The corresponding code methodology and subdivision algorithm for the use of the linear imaging detector are discussed below. Both were found to be highly effective after rigorous testing; the proposed encoder was built accordingly and tested to find that its resolution can reach 1.24″, while the mean-square deviation of its errors is 14.3″. The proposed encoder consistently performed well and returned high-tone despite its compact size.

The remainder of this paper is organized as follows: Section 2 proposes the angular displacement measurement mechanism, Section 3 discusses our technique for encoding the circular grating, and Section 4 discusses our process of building the subdivision model; Section 5 reports our test results on the small photographic encoder, and Section 6 provides a brief summary and conclusion.

2. PRINCIPLE OF ANGULAR DISPLACEMENT MEASUREMENT

The angular displacement measurement technique proposed here recognizes grating patterns with an image sensor and decodes them via digital image processing. We used a light source to irradiate the grating throughout our experiments on angular displacement measurement. Light passes through the grating, and the grating pattern projects onto the image sensors, as shown in Fig. 1.

As depicted in the diagram below, the linear imaging sensor distinguishes the image of the grating disk and yields current code data X; the code data can be transformed to decoding data X' via the decoding table. Subdivision data α is calculated using the subdivision algorithm; we achieved 2^{12}-fold subdivision from the code data. The output binary numbers consist, accordingly, of "decoding data" and "subdivision data." The decoding data X' are 8 bit, and the subdivision data α are 12 bit; the measurement resolution is $360°/2^{20}$.

An appropriate light source is imperative for high-quality image receiving. The light source can be designed in two ways: with an optical lens to change the point light source to a parallel source or with a uniform area source. The parallel source installation is complex, and the manufacturing cost is high; it also generally leads to a bulky device. We designed our optical light guide plate from highly reflective optical acrylic material. The optical light guide plate can change a point light to a uniform area source, as shown in Fig. 1(a). Light irradiates in the profile of the light guide plate and reflects inside the plate, penetrating the guide points carved onto the surface and exiting as uniform light.

The proposed grating disk is shown in Fig. 1(b). The linear imaging sensor code is designed as a single circle, as discussed further in Section 3. The light that passes through the grating is magnified by an optical lens and projected onto the image sensors; the principle of optical amplification is shown in Fig. 1(c).

We set s as the space between the grate and the center of the lens, k as the space between the image detector and the lens, and f as the focal distance of the lens. According to the imaging principle, the relation between the subject distance and the image distance is $1/s + 1/k = 1/f$. The subject height is d, and the image plane height is h. We have $1/s + 1/k = 1/f$. Thus,

$$s = f(1 + d/h), \tag{1}$$

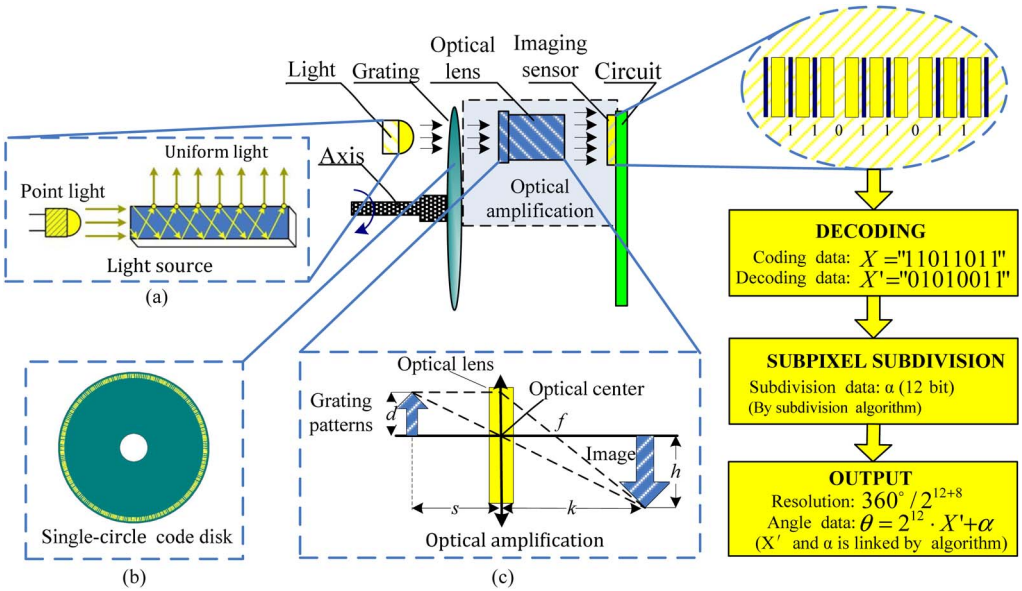

Fig. 1. Angular displacement measurement principle: (a) light source, (b) grating disk, and (c) optical amplification.

$$k = f(1 + h/d). \quad (2)$$

To ensure that a complete 8 bit grating image is received, the image detector must have at least 10 grating grooves. The length of the 10 grating grooves is 4.4 mm when the diameter of the code-grooves circle is 36 mm, so $d = 4.4$ mm. The width of the image sensor $h = 4.9$ mm and $f = 4.0$ mm, so $s = 7.59$ mm and $k = 8.45$ mm.

3. GRATING CODE

Reducing the line density within the maximum limit is the rule of designing small-size grating disks. We used a code mode that ensures high utilization of grating grooves accordingly [21]. We set $X = \{X_1, X_2, \ldots, X_n\}$ as n bit code elements. Binary code values become new code values when the grating rolls in one code resolution. The read encoding values then change from $X_1, X_2, \ldots, X_n$ to $X_2, X_3, \ldots, X_n, X_{n+1}$. Every code value X_i is obtained by the logical operations of former n values $X_{i-n} - X_{i-1}$, as shown in Fig. 2.

In Fig. 2, operation "⊕" means "XOR," X_i is an i code element ("0" or "1"), coefficient a_i is "0" or "1," and a_n is always "1." The rational selection of $a_1 - a_n$ can make the maximum code quantity $2^n - 1$.

We calculated $a_1 - a_n$ in MATLAB to set $\{X_1, X_2, \ldots, X_8\} = \{0, 0, \ldots, 1\}$ at the beginning of the experiment. There are many $a_1 - a_n$ groups that can ensure the code element has maximum quantity. The group we used in this study and the polynomial of the 8 bit code with maximum quantity are shown in Eq. (3) as follows:

$$X_i = X_{i-1} \oplus X_{i-2} \oplus X_{i-3} \oplus X_{i-8}. \quad (3)$$

We designed an 8 bit single absolute encoding on the grating with $\phi 38$ mm diameter and inserted reference lines among encoding lines according to the results of Eq. (3). The reference lines have angle subdivision, as shown in Fig. 3.

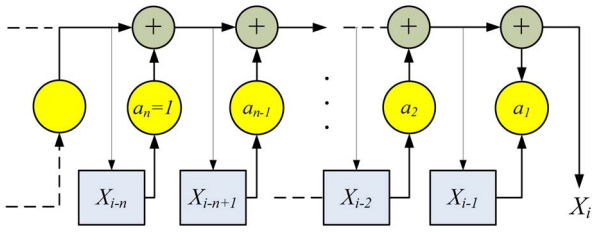

Fig. 2. Principle of the code value.

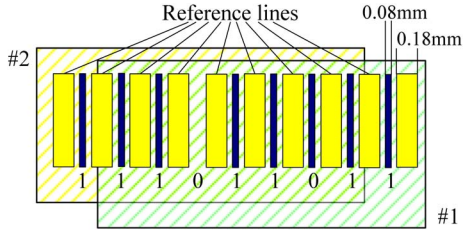

Fig. 3. Partial 8 bit code disk.

Table 1. Partial Decoding Table

No.	Coded Values	Decoding Values
0	00000000	00000000
1	10000000	00000001
⋮	⋮	⋮
80	11011111	01010000
81	01101111	01010001
82	10110111	01010010
83	11011011	01010011
84	11101101	01010100
85	11110110	01010101
86	01111011	01010110
87	10111101	01010111
88	01011110	01011000
89	10101111	01011001
⋮	⋮	⋮
254	00000010	11111110
255	00000001	11111111

In Fig. 3, rectangle #1 is read as "11011011;" rectangle #2 is read as "11101101" after the grate rotates one resolution.

We made a decoding conversion table for decoding in which every code has only one decoding value that changes as the grating disk rolls. A portion of the 8 bit code conversion table is shown in Table 1. Every code value was obtained by the 1 bit right-shifting of the prior code value and addition of X_i. Rectangle #1 in Fig. 5 is "$X = 11011011$," and its decoding value is "$X' = 01010011$ (No. 83);" the code number of rectangle #2 is "$X = 11101101$" and its decoding value is "$X' = 01010100$ (No. 84)."

The linear image sensor can perform decoding functions through its single-circle code or by using one-line pixels of a plane array image sensor.

4. SUBPIXEL SUBDIVISION

A. Subdivision Algorithm

The subpixel subdivision algorithm described here was developed based on the "centroid algorithm." It subdivides the angular displacement between consecutive codes by recognizing reference lines; the subdivision values are called "subdivision codes α." The principle of the subdivision is shown in Fig. 4.

Line AB is linear image sensor information, the y axis is the detection line, and O is the center of the code disk. The y axis intersects two "reference lines" at A and B; line AB intersects the y axis at C, and ∠COB is the measured angle. The A coordinate and B coordinate are the "centroid" of the reference line and can be calculated as follows:

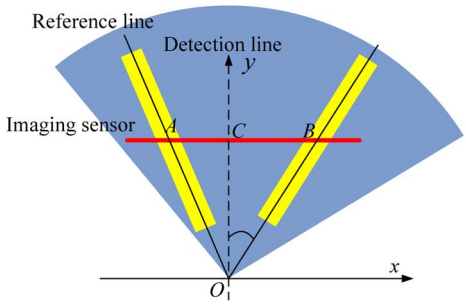

Fig. 4. Principle of the subdivision.

$$U = \sum_{i=1}^{k} P_i G_i / \sum_{i=1}^{k} P_i, \tag{4}$$

where P_i is the value of pixel i, G_i is position of pixel i, and k is the window size. ∠COB can be calculated as follows:

$$\angle \mathrm{COB} = \arctan(CB/y_c). \tag{5}$$

The subdivision value is $\alpha = 2^n \cdot \angle \mathrm{COB}/\angle \mathrm{AOB}$, where n is the bit number of the subdivision values. We set y_c as the reference, but during the experiment, we found that y_c caused errors due to installation and adjustment. In short, Eq. (5) cannot realize high-resolution subdivision.

In Fig. 4, $\angle \mathrm{AOB} = 2\pi/2^m$, where 2^m is the number of reference lines in one circle. When the number of reference lines 2^m is sufficient, AB/CB approximates to $\angle \mathrm{AOB}/\angle \mathrm{COB}$, so ∠COB can be calculated by Eq. (6). The larger 2^m is, the smaller the errors of Eq. (6) are. We have

$$\angle COB \approx \frac{CB}{AB} \cdot \angle AOB; AB = U_A - U_B; CB = U_C - U_B. \tag{6}$$

We let the sum of AB and CB be the comparative reference and CB be subdivision indicated value. When $n = 12$, the 2^{12}-fold subdivision is expressed as follows:

$$\alpha \approx 2^{12} \cdot \frac{CB}{AB}. \tag{7}$$

B. Connection of Decoding Data and Subdivision Data

The angular measurement values are comprised of code numbers and subdivision values, and the output binary data are calculated as $\theta = 2^n \cdot X' + \alpha$. During practical application, the carry and link between decoding data X' and subdivision data α must be appropriately accounted for; here, we did so via the connection algorithm shown in Fig. 5. We set $U1$–$U9$ as the centroids of Y1–Y9 and $U0$ as the center of the detection line.

Generally speaking, the detection line does not overlap the reference lines (line #1 in Fig. 5). The subdivision value is calculated by Eq. (8), and the encoding data are "00101111."

During the grating rotation, the detection does overlap the reference line (line #2 in Fig. 5). We first calculated $U5$ by using Eq. (4) to determine whether $U5$ was on the left side of line #2. If not, the subdivision value was calculated by Eq. (8). If so, it was calculated by Eq. (9), in which case encoding data were "01011110." We have

$$\alpha_1 = 2^n \cdot \frac{U0 - U5}{U4 - U5}, \tag{8}$$

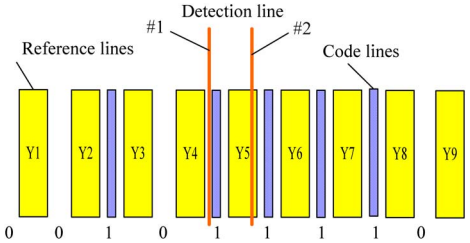

Fig. 5. Connection of the encoding data and subdivision data.

$$\alpha_2 = 2^n \cdot \frac{U0 - U6}{U5 - U6}. \tag{9}$$

5. EXPERIMENTS

We designed an encoder prototype based on the information above. The circuit was designed as an STM32F746 chip that carries a Cortex-M7 core; the image sensor is a linear image sensor with 640 pixels. The focal distance of the lens is 4 mm, the diameter of the encoder is 50 mm, the length of the encoder is 75 mm, the diameter of the grate is 38 mm, and the diameter of the lens is 14 mm. All the devices are shown in Fig. 6.

A. Decoding and Subdivision

We collected four images with the encoder, as shown in Fig. 7. The reference lines are wider than the code lines, which made identifying the 8 bit code lines quite easy. In Fig. 7(a), the coding value is "01100010;" in Fig. 7(b), it is "00101101;" in Fig. 7(c), it is "11110110;" and in Fig. 7(d), it is "11101101." The image is legible for decoding.

To test the subdivision algorithm, we collected the pixel data of the linear image sensor when it was working. Table 2 shows the collection pixel data of reference lines on both sides of the

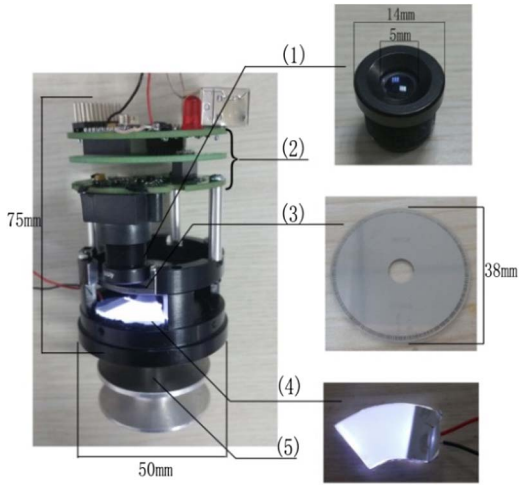

Fig. 6. Experiment: (1) image sensor, (2) coding circuit, (3) code disk, (4) optical lens, and (5) flange.

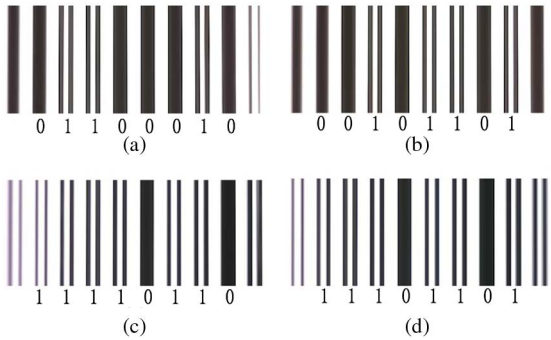

Fig. 7. Data collected.

Table 2. Pixel Data of Reference Lines

First Time				Second Time			
Reference Line A		Reference Line B		Reference Line A'		Reference Line B'	
No.	Pixels	No.	Pixels	No.	Pixels	No.	Pixels
306	0	362	0	306	0	362	0
307	91	363	86	307	90	363	87
308	163	364	246	308	174	364	250
309	186	365	244	309	186	365	236
310	167	366	173	310	168	366	173
311	169	367	177	311	169	367	177
312	170	368	177	312	171	368	177
313	170	369	177	313	171	369	177
314	170	370	177	314	172	370	176
315	170	371	177	315	171	371	177
316	170	372	176	316	171	372	177
317	170	373	176	317	171	373	176
318	169	374	176	318	170	374	177
319	169	375	176	319	170	375	177
320	169	376	177	320	170	376	177
321	169	377	177	321	169	377	177
322	169	378	177	322	169	378	177
323	169	379	178	323	169	379	178
324	168	380	178	324	168	380	178
325	168	381	178	325	168	381	179
326	168	382	178	326	168	382	179
327	168	383	179	327	168	383	180
328	168	384	178	328	168	384	179
329	167	385	174	329	168	385	175
330	161	386	255	330	163	386	255
331	246	387	195	331	243	387	194
332	154	388	82	332	159	388	83
333	55	389	0	333	60	389	0

detection line in two times. Meanwhile, the position of the detection line is 320. By the calculation of Eq. (4), the first time, the centroid of reference line A is $U_A = 319.99$, and the centroid of the reference line B is $U_B = 375.40$. The subdivision fold is set as $2^N = 2^{12}$, so the subdivision value is 0.73 by Eq. (7), which is "0000 0000 0000" in the binary system.

We rotated the axis by a very small amount and collected the pixel data on both sides of the detection line the second time. For the calculation, the centroid of reference line A' is $U_{A'} = 319.98$ and $U_{B'} = 375.41$; the subdivision value is 1.48, which is "0000 0000 0001" in the binary system. It shows that the subdivision algorithm can achieve the 2^{12}-fold subdivision.

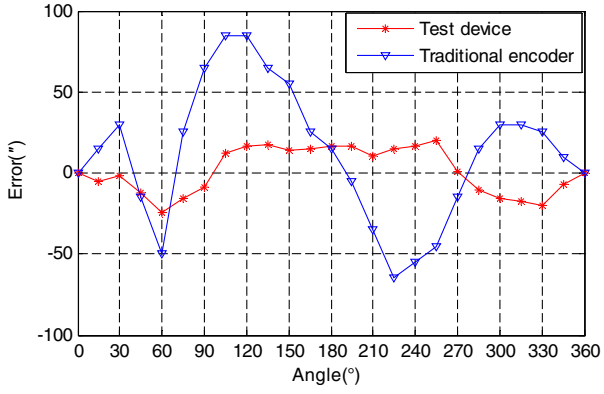

Fig. 8. Measurement errors.

We carefully rotated the principal axis of the test encoder, and the resulting output binary data had no error. When the principal axis was motionless, the output binary number was steady. We achieved 8 bit decoding and 2^{12}-fold subdivision using the proposed device successfully. The resolution of the device is 1.24″ (20 bit).

B. Error Measurement

We measured the test device with a large, 24 bit reference photoelectric encoder with precision of 1″ and resolution of 0.07″. Error was recorded at each 15° point. Simultaneously, we measured a traditional encoder that is the same as the test device in grating diameter. The results are shown in Fig. 8, where the mean-square deviations of the errors are 14.3″ and 41.5″. In effect, the proposed encoder exhibited higher precision than traditional small-size encoders.

6. CONCLUSIONS

This paper has proposed a novel high-resolution angular displacement measurement technology. We first established a new method of angular displacement measurement and then explored the implementation of high-resolution measurement via circular grating disks. We developed a subdivision method based on a subpixel algorithm accordingly. We then built a prototype of the device 50 mm in diameter and tested it to find that it can achieve angular measurement with resolution of 1.24″ and precision below 15″; in short, the proposed device is feasible and effective while outperforming other devices that are similar in size. The results reported here may provide the theoretical and technological foundation for the design of small-size, high-resolution photographic rotary encoders in the future.

Funding. National Natural Science Foundation of China (NSFC) (51605465).

REFERENCES

1. D. Fang, C. Jie, W. Yangyong, and G. Kun, "Measurement and calibration method for an optical encoder based on adaptive differential evolution-Fourier neural networks," Meas. Sci. Technol. **24**, 055008 (2013).
2. K. Hane, T. Endo, M. Ishimori, and M. Sasaki, "Integration of grating-image-type encoder using Si micromachining," Sens. Actuators A **97–98**, 139–146 (2002).
3. Z. Hongbo, W. Qiuhua, W. Shujie, Y. Hai, and L. Lihui, "Installation error control of dynamic measurement for small photoelectric encoder," Opt. Precis. Eng. **24**, 1655–1660 (2016), in Chinese.
4. Y. Hai, W. Qiuhua, L. Xinran, Z. Changhai, and L. Lihui, "Calibration of dynamic precision for measurement platform of photoelectric encoder," Opt. Precis. Eng. **24**, 87–92 (2016), in Chinese.
5. C.-F. Kao, H.-L. Huang, and S.-H. Lu, "Optical encoder based on fractional-Talbot effect using two-dimensional phase grating," Opt. Commun. **283**, 1950–1955 (2010).
6. D. Mancini, E. Cascone, and P. Schipani, "Galileo high-resolution encoder system," Proc. SPIE **3112**, 328–334 (1997).
7. W. Luo, Y. Zhang, A. Feizi, Z. Gorocs, and A. Ozcan, "Pixel super-resolution using wavelength scanning," Light Sci. Appl. **5**, e16060 (2016).
8. J. Qin, R. M. Silver, B. M. Barnes, H. Zhou, R. G. Dixson, and M.-A. Henn, "Deep subwavelength nanometric image reconstruction using

Fourier domain optical normalization," Light Sci. Appl. **5**, e16038 (2016).
9. S. Witte, V. T. Tenner, D. W. E. Noom, and K. S. E. Eikema, "Lensless diffractive imaging with ultra-broadband table-top sources: from infrared to extreme-ultraviolet wavelengths," Light Sci. Appl. **3**, e163 (2014).
10. A. C. Sobieranski, F. Inci, H. C. Tekin, M. Yuksekkaya, E. Comunello, D. Cobra, A. von Wangenheim, and U. Demirci, "Portable lensless wide-field microscopy imaging platform based on digital inline holography and multi-frame pixel super-resolution," Light Sci. Appl. **4**, e346 (2015).
11. K. Patorsky and M. Kujawinska, *Handbook of the Moiré Fringe Technique [M]* (Elsevier, 1993).
12. D. B. Leviton and B. J. Frey, "Ultra-high resolution, absolute position sensors for cryostatic applications," Proc. SPIE **4850**, 776–787 (2003).
13. D. B. Leviton and M. S. Garza, "Recent advances and applications for NASA's new, ultra-high sensitivity, absolute, optical pattern recognition encoders," Proc. SPIE **4091**, 375–384 (2000).
14. J. S. Bajić, D. Z. Stupar, B. M. Dakić, M. B. Živanov, and L. F. Nagy, "An absolute rotary position sensor based on cylindrical coordinate color space transformation [J]," Sens. Actuators A **213**, 27–34 (2014).
15. Y. Sugiyam, Y. Matsu, H. Toyod, N. Mukozaka, A. Ihori, T. Abe, M. Takabe, and S. Mizuno, "A 3.2 kHz 14-bit optical absolute rotary encoder with a CMOS profile sensor," IEEE Sens. J. **8**, 1430–1436 (2008).
16. M. Tresanchez, T. Pallejà, M. Teixidó, and J. Palacín, "Using the image acquisition capabilities of the optical mouse sensor to build an absolute rotary encoder," Sens. Actuators A **157**, 161–167 (2010).
17. J.-A. Kim, J. W. Kim, C.-S. Kang, J. Jin, and T. B. Eom, "Absolute angle measurement using a phase-encoded binary graduated disk," Measurement **80**, 288–293 (2016).
18. Y.-N. Wang, B. Yaun, and X.-X. Ni, "Subdivision technique of absolute angular encoder using array detector," J. Chin. Zhejiang Univ. (Engineering Science) **45**, 370–374 (2011), in Chinese.
19. M. Hongrui, "Study on integrated application of rangefinder and electronic theodolite and key technologies," Master's thesis (Chinese Nanjing University of Science and Technology, 2013), pp. 4–17.
20. Q. Lili, "Angle-measurement technology of an optical pattern rotary encoder and its hardware implementation," Acta Opt. Sin. **33**, 0412001 (2013), in Chinese.
21. D. Yingcai, S. Lu, W. Qiuhua, and Y. Hai, "Design of high resolution absolute code disk based on allegro image discriminate," Acta Opt. Sin. **36**, 1112001 (2016), in Chinese.